ACS Combinatorial Science

RESEARCH ARTICLE

pubs.acs.org/acscombsci

High-Throughput Method to Study the Effect of Precursors and Temperature, Applied to the Synthesis of $LiNi_{1/3}Co_{1/3}Mn_{1/3}O_2$ for Lithium Batteries

Matthew Roberts,* and John Owen

School of Chemistry, University of Southampton, Southampton, Hampshire, SO17 1BJ, U.K.

ABSTRACT: This paper presents a new technique for the high-throughput investigation of preparation conditions of new materials. The method allows for the investigation of different starting materials as a function of the synthesis temperature. This is a novel area for high-throughput work, derived from the Post Synthesis Array Transfer (PoSAT) method. This new application of the PoSAT method was then used to investigate a number of different preparation conditions of $LiNi_{1/3}Co_{1/3}Mn_{1/3}O_2$ within a temperature gradient. As a result of this work, new, facile synthesis conditions (from an aqueous solution of mixed metal nitrates, dried and then calcined at 700 °C) for $LiNi_{1/3}Co_{1/3}Mn_{1/3}O_2$ material were identified to provide a competitive electrochemical performance (140 mA h g^{-1} stable capacity when cycled in the potential window 2 to 4.2 V at). This work has also highlighted how sensitive this material is to the powder morphology.

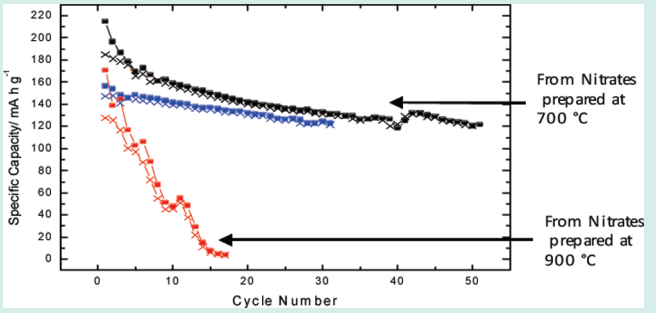

KEYWORDS: lithium, battery, high-throughput, $LiNi_{1/3}Co_{1/3}Mn_{1/3}O_2$, cathode

INTRODUCTION

High throughput methods for synthesis and testing of battery electrodes have recently enabled the rapid discovery of new materials.[1] By contrast with traditional methods which involve synthesis, characterization, and testing of one material at a time, the high throughput approach is to fabricate an array of many different samples to be characterized and tested in parallel.[2,3] Physical vapor deposition has been very successful for preparations of large area thin films of ternary metal alloy samples covering wide composition ranges.[4] The results of such studies have identified new negative electrodes with enhanced capacity for lithium storage, for example, Si−Al−Mn[5] and other alloy systems.[6] Other high-throughput battery studies include preparation by electrolytic deposition of MnO_2[7] and doped lithium titanates.[8]

Over the past 30 years of lithium ion battery research synthesis conditions have shown themselves to be extremely important in obtaining optimal performance of a given material. Each time a promising new material has been proposed many papers have been presented which show different synthetic routes to the same material each resulting in varied performance (e.g., $LiFePO_4$[9−11]). These papers usually investigate different synthesis temperatures and different precursor salts. Therefore the discovery of new lithium battery materials will benefit from high-throughput studies of the effect of temperature as in other fields, for example, the work of Portyrailo et al., which describes a method to view the effect of annealing temperatures of up to 140 °C on polymeric sensing materials.[12]

The $LiNi_{1/3}Co_{1/3}Mn_{1/3}O_2$ was proposed in 2001 by Ohzuku et al.[13,14] as a high voltage cathode (discharging around 4 V vs Li). Capacities greater than 200 mA h g^{-1} have been reported for this material in the range 2 to 4.6 V with negligible capacity loss.[14,15] Ohzuku et al. propose that in the $LiNi_{1/3}Co_{1/3}Mn_{1/3}O_2$ structure the Co, Ni, and Mn exist in the 3+, 2+, and 4+ oxidation states, respectively.[16] The charging reaction is shown below in eq 1. However, the theoretical capacity of 278 mA h g^{-1} according to this equation has not be observed within the potential limits of most experiments.

$$LiNi_{1/3}Co_{1/3}Mn_{1/3}O_2 \leftrightarrow Ni_{1/3}Co_{1/3}Mn_{1/3}O_2 + Li^+ + e^- \quad (1)$$

This material has other advantages over $LiCoO_2$, for example, the reduction of Co results in a reduction in cost and toxicity. However, several reports in the literature have shown that while structurally pure materials have been obtained it has been difficult to reproduce the electrochemical performance.[17−19] The main preparation routes have been to precipitate either the metal hydroxides or the metal carbonates from a solution of the metal sulphates or nitrates, although many other routes have been tried. It is apparent from these studies that the preparation of this material is sensitive to reaction conditions such as calcinations temperature and time, precursor salts,[15,18,19] and also the use of excess Li seems to be important. One of the most

Received: October 5, 2010
Revised: October 22, 2010
Published: November 18, 2010

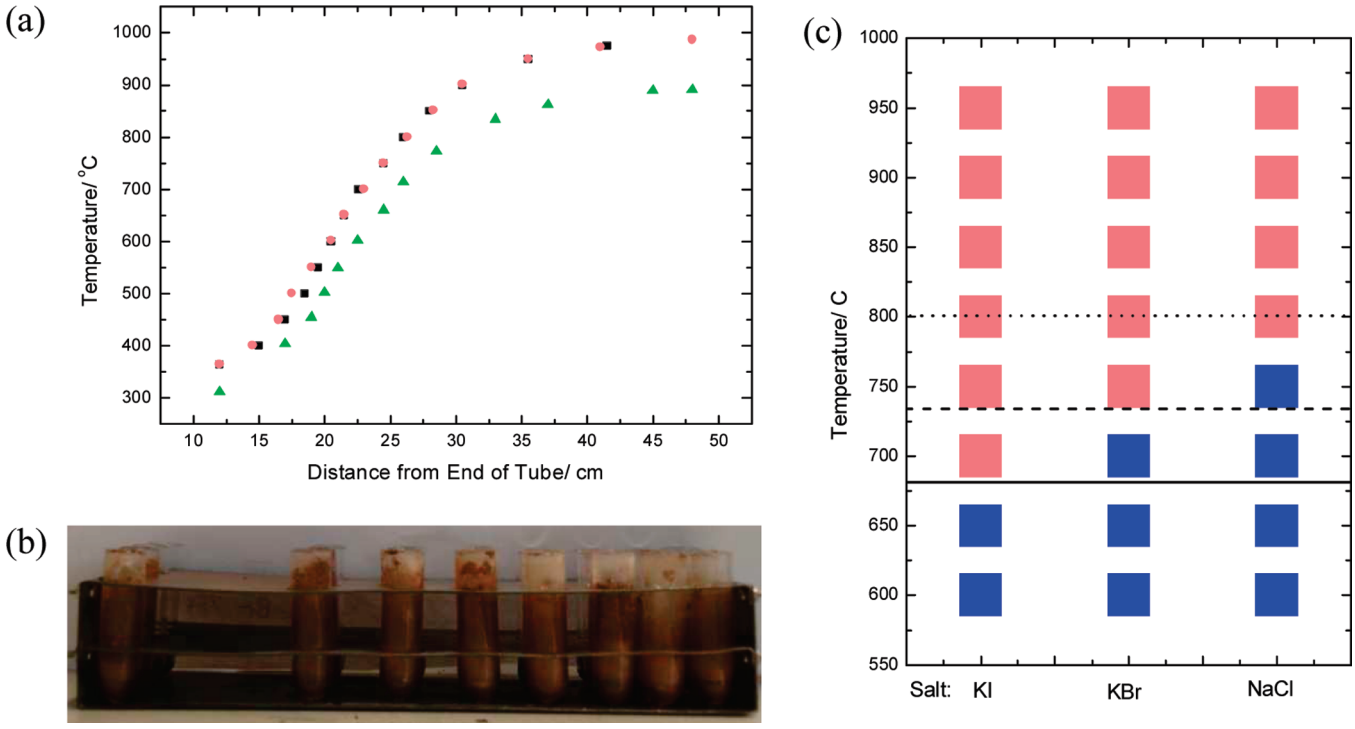

Figure 1. (a) Temperature gradient from the end of the tube 1000 °C run 1 (black solid squares), 1000 °C run 2 (red solid circles), and 900 °C (green solid triangles). (b) HT Furnace Rack. (c) Representation of salt melting experiment, the temperature scale indicates the conditions expected. Colored squares show samples which remained solid (blue solid squares) and samples which melted (red solid squares). Also shown are the lines indicating the known melting points for NaCl (dotted line), KBr (dashed line), and KI (solid line).

promising synthesis methods has been proposed by Shaju et al. who prepared a macroporous $LiNi_{1/3}Co_{1/3}Mn_{1/3}O_2$ using a dilute solution of metal acetates mixed with resorcinol and formaldehyde in a sol−gel method.[15] This material shows a 99.9% retention of capacity per cycle compared with the best reported elsewhere of 99.83% and it also shows a high rate capability. The excellent performance of this material was attributed to an optimized powder morphology.[15] Other methods to improve the performance of this material have used a variety of surface treatments[20,21] to improve the retention of capacity on cycling and also cationic substitution.[22,23] Recently, Thackeray et al.[24] have shown that by washing the $LiNi_{1/3}Co_{1/3}Mn_{1/3}O_2$ in a dilute solution of NH_4PF_6 prior to testing a significant improvement in the retention of capacity on cycling can be achieved.

The aims of the work are as follows:

- To adapt our Post Synthesis Array Transfer (PoSAT) method to the study of thermally graded arrays.
- To prove the concept of this new method with an investigation of the effect of different preparation conditions on $LiNi_{1/3}Co_{1/3}Mn_{1/3}O_2$.
- To identify a simple solution based method for the synthesis of $LiNi_{1/3}Co_{1/3}Mn_{1/3}O_2$.

EXPERIMENTAL SECTION

Measuring the Thermal Gradient within the Tube Furnace. To measure the temperature gradient within the tube furnace (Lenton) a hole was drilled in one of the stainless steel end stoppers and through one of the thermal bungs. A thermocouple was then inserted during heating and moved to different positions to record the temperature (the thermocouple was left at each position for 10 min to equilibrate before measurement). The furnace controller was then set to temperatures of 900 and 1000 °C (on two separate runs) with the furnace internal sensor placed at a central position, with a heating rate of 5 °C min^{-1} and a gas flow rate of 0.5 L min^{-1}. The furnace was left to equilibrate for 2 h before any measurements were made.

Validation of the Thermal Gradient within the Tube Furnace. Three salts were chosen NaCl (Aldrich), KBr (Aldrich) and KI (Aldrich) with melting points 800.8, 734, 681 °C. 0.5 g samples of salt were placed in each quartz tube so that three columns of the rack were utilized, each column containing a different salt. These tubes were then heated in the thermal gradient by placing them in a rack designed (shown in Figure 1b) to locate the array across the gradient at 18.5 cm into the tube. This rack is designed so that when placed with the right end 18.5 cm into the furnace the rows of the array will be exposed to 600, 650, 700, 750, 800, 850, 900, and 950 °C. This rack can only accommodate 32 tubes, and the synthesis will have to be performed twice to prepare all 64 samples in a standard array. The furnace controller was set to 1000 °C, with a heating rate of 5 °C min^{-1} and an Ar gas flow rate of 0.5 L min^{-1} was applied.

Electrode Array Preparation by PoSAT. Solutions of $LiCH_3COO$ (2.5 M, 250 mL), $Co(NO_3)_2 \cdot 6H_2O$ (1.25 M, 250 mL), $Ni(NO_3)_2 \cdot 6H_2O$ (1.25 M, 250 mL), $Mn(NO_3)_2 \cdot 6H_2O$ (Alfa Aesar, 1.25 M, 250 mL), $Ni(CH_3COO)_2 \cdot 4H_2O$ (0.625 M, 250 mL), $Mn(CH_3COO)_2$ (0.625 M, 250 mL), $Co(CH_3COO)_2 \cdot 4H_2O$ (0.625 M, 250 mL), sucrose (2 M, 100 mL), ammonium hydroxide (28 wt % aqueous solutions, 100 mL), Brij 78 (4 wt % aqueous solutions, 100 mL, referred to as just Brij), ethylene glycol and citric acid (2 M, 100 mL) were prepared. The precursor salt solutions were then mixed as shown in Table 1 with metal ratios as defined in the formula $LiNi_{1/3}Co_{1/3}Mn_{1/3}O_2$ by

dx.doi.org/10.1021/co100028m |ACS Comb. Sci. 2011, 13, 126–134

Table 1. Table Showing the Preparation Mixtures Used to Prepare $LiNi_{1/3}Co_{1/3}Mn_{1/3}O_2$[a]

	array	columns	precursors salts	precipitation additive	additive to stop crystallization
nitrates only	1	1, 2	$LiCH_3COO$, $Ni(NO_3)_2$, $Mn(NO_3)_2$, $Co(NO_3)_2$		
nitrates + sucrose	1	3, 4	$LiCH_3COO$, $Ni(NO_3)_2$, $Mn(NO_3)_2$, $Co(NO_3)_2$		31.2 μL of 1 M sucrose
hydroxide	1	5, 6	$LiCH_3COO$, $Ni(NO_3)_2$, $Mn(NO_3)_2$, $Co(NO_3)_2$	0.473 mL of 28% ammonium hydroxide	
EG citrate	1	7, 8	$LiCH_3COO$, $Ni(NO_3)_2$, $Mn(NO_3)_2$, $Co(NO_3)_2$		70 μL of ethylene glycol and 0.625 mL of 2 M citric acid
Brij	2	1, 2	$LiCH_3COO$, $Ni(NO_3)_2$, $Mn(NO_3)_2$, $Co(NO_3)_2$		1 mL of 4 wt % aqueous Brij 78
Brij + EG and citrate	2	3, 4	$LiCH_3COO$, $Ni(NO_3)_2$, $Mn(NO_3)_2$, $Co(NO_3)_2$		1 mL of 4 wt % aqueous Brij 78, 70 μL of ethylene glycol, and 0.625 mL of 2 M citric acid
acetates only	2	5, 6	$LiCH_3COO$, $Ni(CH_3COO)_2$, $Mn(CH_3COO)_2$, $Co(CH_3COO)_2$		
acetates + sucrose	2	7, 8	$LiCH_3COO$, $Ni(CH_3COO)_2$, $Mn(CH_3COO)_2$, $Co(CH_3COO)_2$		31.2 μL of 1 M sucrose

[a] Total volume of precursor salt solutions 1 mL.

the automated liquid handling robot (Perkin-Elmer Life Sciences). Using hand automated pipettes the various additives were then dispensed into the appropriate positions on the array. In the case of the hydroxide precipitation method, small (4 × 2 mm) magnetic stirrer bars were added to each tube prior to the ammonia hydroxide addition. The solutions were then stirred at 60 °C for 12 h after the addition of ammonium hydroxide to each tube. For the ethylene glycol and citric acid[25] preparations the additive was dispensed at room temperature and the samples were then heated to 90 °C for 10 min and then 40 °C for 10 h. In all other preparations the samples were simply dried to solids at 60 °C. Then 32 precursors at a time were placed within a rack designed to utilize the thermal gradient in the tube furnace such that each row in the array was exposed to a different temperature; 600, 650, 700, 750, 800, 850, 900, and 950 °C. This synthesis was performed in a pure oxygen atmosphere. After cooling, the products were crushed by adding five 1 mm zirconia beads to each tube followed by placing the whole array on a vibrating table (IKA VIBRAX VXR Basic). Composite electrode preparation began by adding two inks, 4% PVdF-HFP (Aldrich, polyvinylidene fluoride-co-hexafluoropropylene) and 4% AB (acetylene black, Shawinigan, Chevron Phillips Chemical Company LP) in cyclopentanone (CP) to the active material powders in each tube. The inks were added to give a final mass ratio of 10% PVdF-HFP, 25% AB, and 65% active material and then mixed using the vortex mixer. Then 14 μL aliquots of each ink were deposited onto the appropriate position on the array of aluminum current collectors and spread across the surface to form an even film of ink. At the same time, a 40 μL sample of each ink was deposited into an array of alumina microcrucibles for thermo gravimetric analysis as detailed below. The CP was evaporated from both arrays at room temperature before drying at 80 °C followed by evacuation. The samples on both arrays were then accurately weighed using a computer monitored balance.

Determination of Active Masses by Thermogravimetric Analysis. The array of samples deposited in alumina microcrucibles was heated to 800 °C in air to burn off carbon and the binder. After allowing the array to cool to room temperature, each sample was weighed again to accurately measure the mass remaining of active material. The percentage of active materials in each element of the electrode array was calculated by assuming that the compositions of samples were identical with corresponding positions in the two arrays.

High Throughput X-ray Diffraction (XRD). For the X-ray phase analysis, we used a combinatorial X-ray diffractometer (Bruker AXS C2, Cu $K_{\alpha 1}$ radiation) that automatically records X-ray patterns of the 64 composite electrodes using a general area diffraction detection system (GADDS). The scan time was 20 min for each sample, that is, about 24 h to record diffraction patterns across the whole array.

High Throughput Electrochemical Evaluation of 64 Electrode Arrays. The cell construction and instrumentation has been reported previously.[2,26] The electrode array was cycled between 2.5 and 4.2 V versus Li at a scan rate of 0.05 mV s^{-1}. Cycling was performed at room temperature (~20 °C).

Bulk Sample Preparation. Samples of $LiNi_{1/3}Co_{1/3}Mn_{1/3}O_2$ were prepared via the nitrate-only method using the same solutions and mixing ratios as that used for the PoSAT array, except that the solution volumes were scaled up to a total precursor volume of 20 mL. Two samples were prepared, and in each case the solution was then dehydrated to leave solid precursors. These two samples were then heat treated at 700 and 900 °C for 10 h in flowing air 0.5 L min^{-1} respectively.

X-ray Phase Analysis on Bulk Samples. X-ray powder diffraction patterns were recorded for the bulk samples using a Bruker D5000 diffractometer. X-ray patterns were collected for the 2θ between 15 and 50° at a scanning rate of about 0.07°/min using a Cu $K\alpha_1$ radiation.

Scanning Electron Microscopy on Bulk Samples. Samples of the active materials were studied by scanning electron microscopy (SEM) using a Philips XL30ESEM at an accelerating voltage between 10 and 15 kV using the secondary electron and backscattered electron detectors.

Electrochemical Testing of Bulk Samples. Electrode film pellets containing 75 wt % of active material, 20 wt % of acetylene black (Shawinigan Black, 100%-compressed, Chevron AB), and 5 wt % poly(tetrafluoroethylene) (PTFE, Type: 6C−N, DuPont) binder were prepared as described previously.[27] The mass of the pellets was in the range 13−17 mg, with a thickness in the range 0.08−0.11 mm. Two-electrode cells were assembled in an argon-filled glovebox (H_2O, O_2 < 1 ppm; Unilab from MBraun). Lithium foil was used as both the counter and the reference electrode, and 1 M $LiPF_6$ in ethylene carbonate/dimethyl

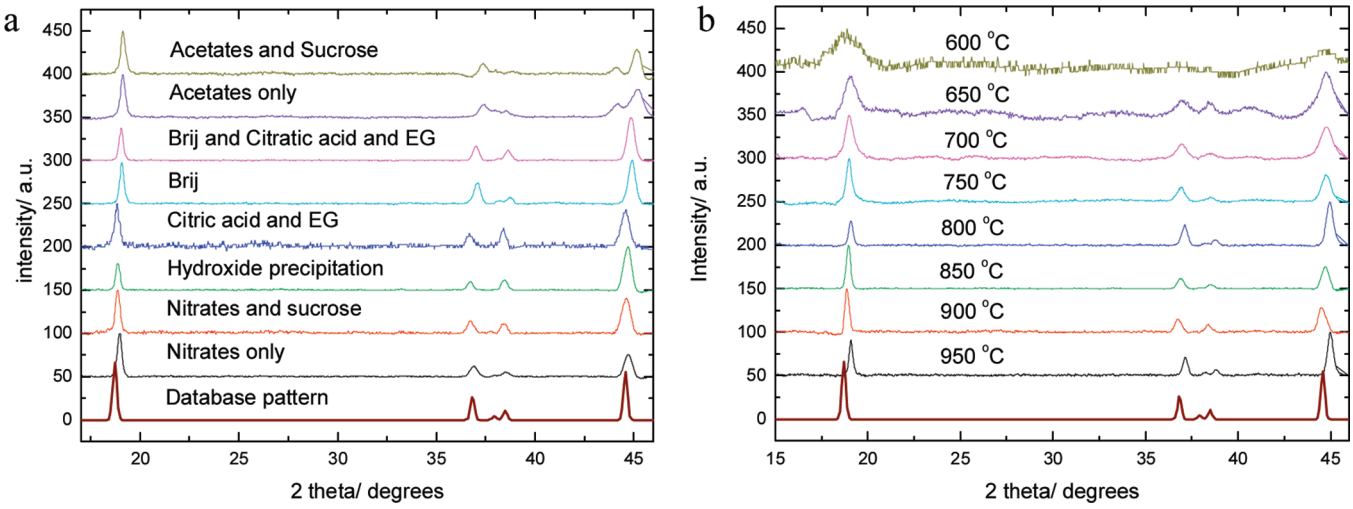

Figure 2. XRD patterns of (a) $LiNi_{1/3}Co_{1/3}Mn_{1/3}O_2$ prepared at 800 °C using the following precursors nitrates only (black line), nitrates with sucrose (red line), hydroxides (green line), citrates and EG (blue line), Brij (aqua line), Brij with citrates and EG (magenta line), acetates only (purple line), and acetates and sucrose (dark olive green line)[6] and (b) $LiNi_{1/3}Co_{1/3}Mn_{1/3}O_2$ prepared via the nitrates only preparation method at 600 (dark olive green line), 650(purple line), 700(magenta line), 750 (aqua line), 800 (blue line), 850 (green line), 900 (red line), and 950 °C (black line). Also shown for comparison is a database result (brown line).[6]

carbonate (EC/DMC: 1/1 by weight, LP30, Merck) as the electrolyte soaked in two glass-fiber separators (GF/F, Whatman). Sandwiched cell materials were compressed in spring-loaded stainless steel cell holders.[28] The cells were cycled galvanostatically at a range of different currents between 2.0 and 4.5 V versus Li using a 16-channel potentiostat (VMP, Princeton Applied Research; Biologic-Science Instruments). Cycling was performed at room temperature (~20 °C).

RESULTS AND DISCUSSION

Measurement of Thermal Gradient within Tube Furnace. The temperature profiles along the tube furnace for set temperatures of 900 and 1000 °C are shown in Figure 1a. Both show a gradual increase from the edge of the furnace to the center. When the target temperature was set to 1000 °C the two repeat measurements can be seen to be in good agreement.

On the basis of the measurements in Figure 1a a special rack was designed which is shown in Figure 1b.

Validation of the Thermal Gradient within the Tube Furnace. The results from the validation of the HT furnace technique are shown in a color map in Figure 1c. It was determined that a sample had melted if it had changed from its original granular appearance to a single transparent solid after heating. It can clearly be seen that the samples were exposed to the expected temperatures. This technique therefore seems suitable for the preparation of temperature graded arrays.

Study on a System Known to Be Sensitive to Preparation Conditions $LiNi_{1/3}Co_{1/3}Mn_{1/3}O_2$

Properties of the Dried Precursors. All precursor solutions started as homogeneous transparent purple solutions. However, after dehydration the properties of the precursor solids varied significantly. In the case of the nitrates only (A), acetates (G), and acetates with sucrose (H) preparations, homogeneous dense purple solids were formed after drying. When nitrates and sucrose (B) were used, a homogeneous porous brown solid was formed. When the hydroxides were precipitated a fine black powder coated the side of the tube. The ethylene glycol citric acid

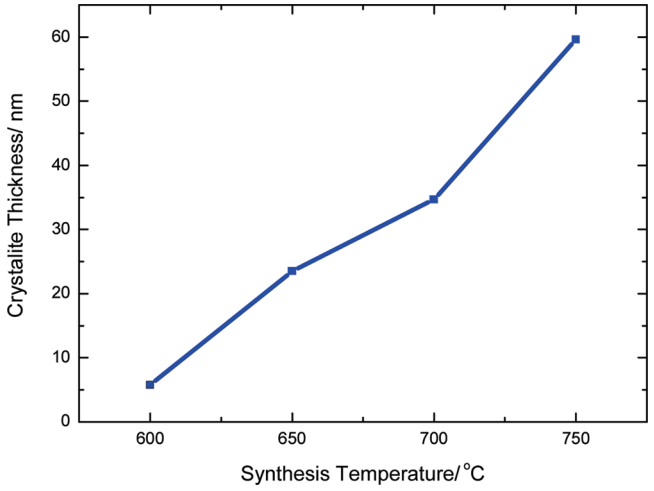

Figure 3. Crystallite thickness of $LiNi_{1/3}Co_{1/3}Mn_{1/3}O_2$ when calcined at different temperatures.

preparation (D) formed a brown gel as the chelating citric acid bound to the metal ions before polymerizing with the ethylene glycol. After high temperature calcinations no visual difference could be seen between any of the samples.

High-Throughput XRD Analysis. The XRD patterns measured for the array composite electrodes for the 800 °C preparations are representative of the trends seen for all synthesis temperatures and are shown in Figure 2a. All patterns except those belonging to the acetates and acetates with sucrose preparations correspond to pure $LiCo_{1/3}Ni_{1/3}Mn_{1/3}O_2$. In the acetate preparations an unidentified impurity peak ($2\theta = 43.5°$) can be seen. This may have been due to a lack of precursor homogeneity, as the manganese acetate is unstable in solution, forming a dark brown precipitate. For several of the patterns the relative intensities of the peaks at ~38° and 45° do not correspond well with the database pattern. The inconsistency is attributed to a peak at 38° due to the PVdF-HFP binder material

dx.doi.org/10.1021/co100028m |ACS Comb. Sci. 2011, 13, 126–134

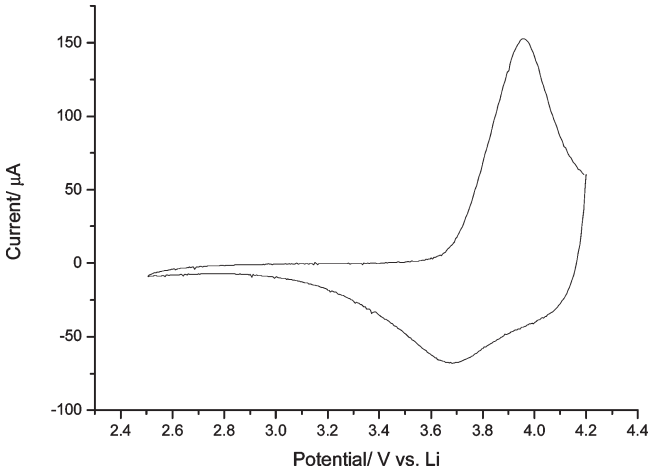

Figure 4. Typical first cycle CV recorded for the materials prepared on both arrays. CV recorded at 0.05 mV s^{-1}.

present in all electrodes, and a peak at 45° due to the aluminum in the substrate below. Small peak shifts between samples were caused by slight variations in sample height during measurement a result of the high-throughput approach and therefore do not indicate differences in lattice parameters.

XRD patterns for all temperature preparations using the nitrate only method are shown in Figure 2b. This is representative of the patterns obtained for each different route. In Figure 2b no detectable impurity peaks are seen in any of the samples. In some samples additional peaks from Al and PVdF-HFP can be seen as before in Figure 2a. The most significant variation is the line broadening for preparations below 800 °C; this effect is typically reported as a reduction in the crystallite size[29,30] because of the slower crystal growth rate at lower temperatures. Using the Scherrer formula (eq 2) this broadening can be interpreted to give the crystallite size as shown in Figure 3.

$$t = \frac{0.9\lambda}{B \cos \theta_B} \quad (2)$$

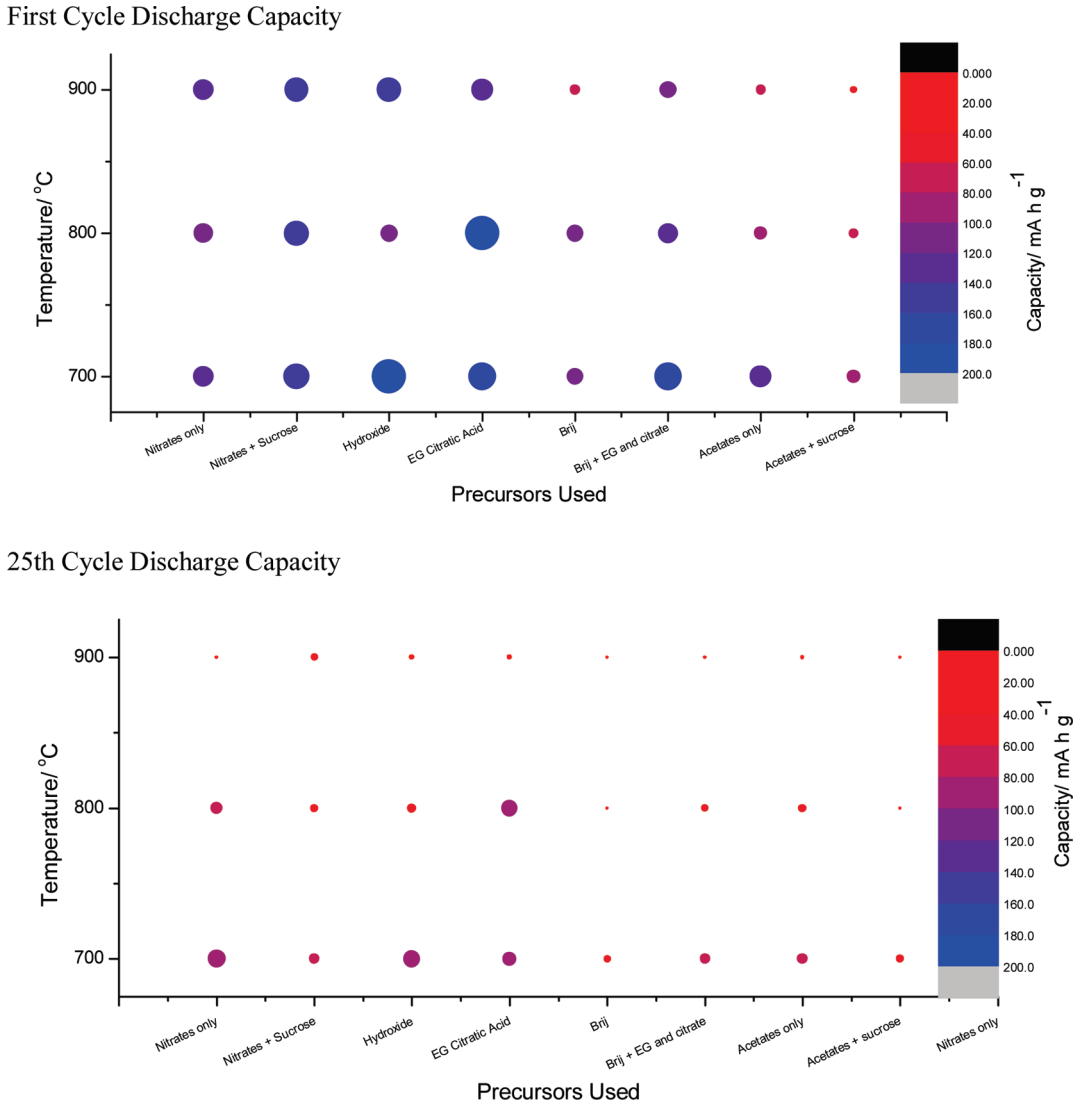

Figure 5. Bubble color maps showing the capacity after the 1st and 25th cycles for the materials on the array shown as a function of both precursors and calcination temperature.

dx.doi.org/10.1021/co100028m |*ACS Comb. Sci.* 2011, 13, 126–134

where t is the crystal size (Å), λ is the X-ray wavelength (Å), θ_B is the Bragg angle, and B is the line broadening in radians at half the maximum intensity

High-Throughput Electrochemical Measurements. A typical cyclic voltammogram (CV; scan rate 0.05 mV s^{-1}) is shown in Figure 4. In general the CVs showed a charge discharge peak around 4 V which is characteristic for this material.[13] The peak shape is characteristic of a redox process without phase change with the charge and discharge peaks occurring in the same voltage range.[31]

To quantify the performance of these materials the discharge capacity per cycle was calculated and the capacity for the first and twentieth cycles are shown in Figure 5 as a color bubble map (here the value of the capacity is shown by the color and size of the point). The duplicate samples on the array were used to average this result so as to reduce the error; only the 700, 800, and 900 °C preparations are shown for simplicity. The initial capacities shown for the materials vary from 60 to 240 mA h g^{-1}, the highest being seen for the hydroxide precipitated materials synthesized at 700 °C. Typically values of 200 mA h g^{-1} are quoted within the literature;[13,15] however, this is normally seen when charging the material to 4.6 V rather than the limited voltage range used in this work. The restricted charging voltage was chosen to minimize any structural damage at high voltage, which may limit cycle life in some materials, for example, $LiCoO_2$.[32] The cycle life of this material is of particular interest as it is indicated in the literature to be the most significant drawback of this material.[17,33,34] Figure 8 shows that the capacity retention of materials prepared at 900 °C is extremely poor; all materials dropping below 40 mA h g^{-1} after 25 cycles—this was also true for the materials prepared at 950 and 850 °C (not shown). The materials synthesized at 800 °C also show a significant, however, less dramatic capacity loss, the best performing of which are the nitrate-only and EG and citrate preparations but still only retain 60 mA h g^{-1} after 25 cycles. The materials synthesized at 700 °C show the highest retention on cycling, the best of which were the nitrate-only (90 mA h g^{-1} after 30 cycles), hydroxide precipitation (110 mA h g^{-1} after 25 cycles), and EG and citric acid (80 mA h g^{-1}) preparations. Of these materials the hydroxide and EG and citric acid preparation show significant capacity losses during the 25 cycles, the high initial capacities leads to the high final capacity. However, the nitrate-only preparation has a maximum capacity of 130 mA h g^{-1} and a final capacity of 90 mA h g^{-1} making its retention of capacity per cycle the highest of any of the materials prepared by the various synthetic routes.

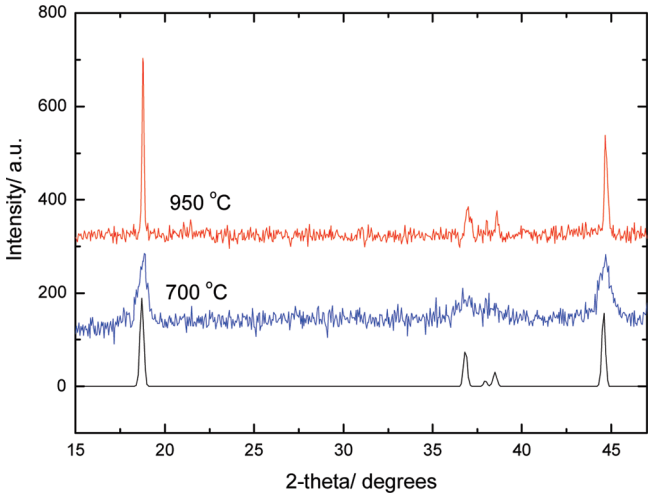

Figure 6. XRD patterns of nitrate only prepared $LiNi_{1/3}Co_{1/3}Mn_{1/3}O_2$ synthesized at both 950 and 700 °C indicated on the graph. Also shown for comparison is a pattern from the literature.[35]

Characterization of Bulk Samples. The aim was to find a simple synthetic route (which could be used to study this mixed metal oxide in future high-throughput studies of compositional variation) which gave a material with a good electrochemical performance. In terms of retention of initial capacity on cycling the nitrate-only, hydroxide precipitation and EG and citric acid method at 700 °C performed the best. However, in terms of the preparation simplicity the nitrates only mixing method is the most straightforward and most suitable for further compositional studies using the high-throughput methods. The reason the hydroxide preparation in particular was discounted at this point (when the results above appear to be the best) is because of the difficulty of using stirrer bars in all 64 samples on the array as required for the preparation. To confirm the performance of the nitrate materials some bulk samples of $LiNi_{1/3}Co_{1/3}Mn_{1/3}O_2$

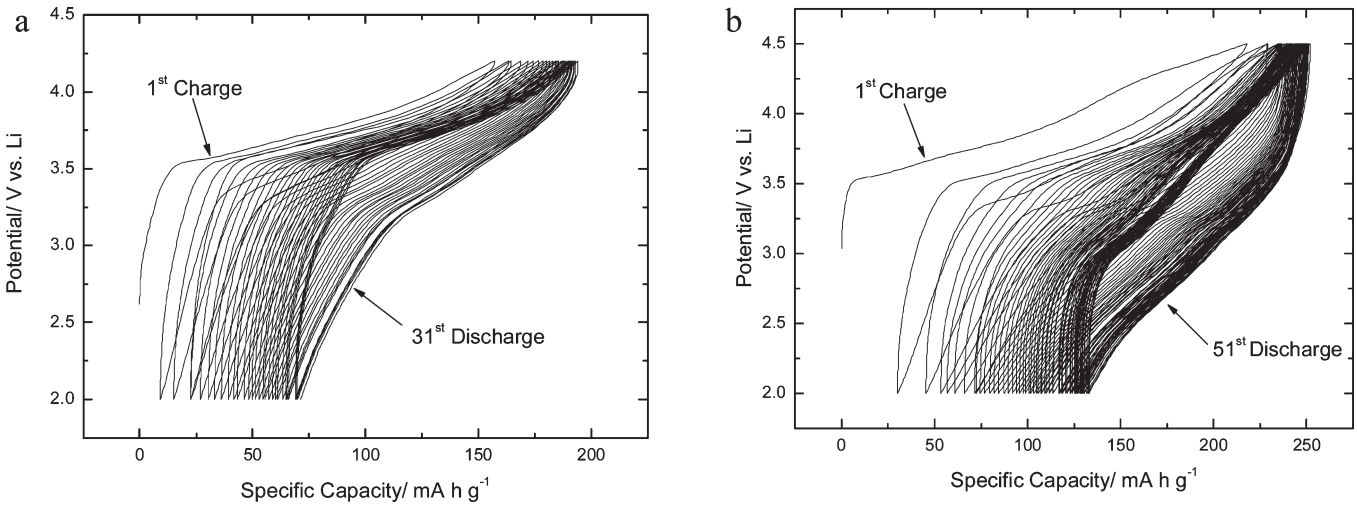

Figure 7. Galvanostatic cycling profile (C/7) for $LiNi_{1/3}Co_{1/3}Mn_{1/3}O_2$ prepared from nitrate only precursor at 700 °C with a upper potential limit of (a) 4.2 V and (b) 4.5 V.

dx.doi.org/10.1021/co100028m |ACS Comb. Sci. 2011, 13, 126–134

were prepared using the nitrate-only preparation method at both 700 and 950 °C.

The XRD patterns in Figure 6 show that there are no detectable impurity peaks in either material as seen in the high-throughput measurements. The same line broadening in the sample prepared at only 700 °C is also seen.

The galvanostatic cycling data for the experiments taken to the potential limits 4.2 and 4.5 V are shown in Figure 7 to illustrate the effect that depth of charge has on the cyclability. In Figure 7a the material shows an initial discharge capacity of 146 mA h g^{-1} which drops to 121 mA h g^{-1} by the 32nd cycle. The shape of the charging curve stays consistent for all cycles, with an area of activity seen above 3.6 V during which approximately 75% of the charging capacity is delivered. There is a significant hysteresis between charge and discharge curve seen in Figure 7a which gets larger on increased cycling. During discharge a voltage plateau can be seen between approximately 4.2 and 3 V where around 60% of the discharge capacity is delivered and then around 40% of the capacity is seen at lower potentials; this general shape is maintained for all 30 cycles.

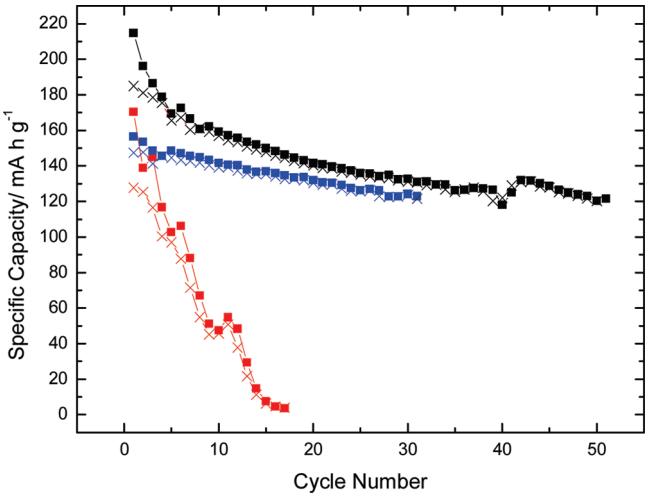

Figure 8. Retention of capacity on cycling for $LiNi_{1/3}Co_{1/3}Mn_{1/3}O_2$ prepared at 700 °C (charged to 4.2 V (blue solid square) and discharged to 2 V (blue times symbol) and charged to 4.5 V (black solid square) and discharged to 2 V (black times symbol)) and 950 °C (charged to 4.5 V (red solid square) and discharged to 2 V(red times symbol)).

The galvanostatic cycling data in Figure 7b shows a marked change from the restricted potential window cycling seen in Figure 7a. Initially a similar voltage charge plateau is seen between 3.5 and 4.5 V; however, over the subsequent 10 cycles this plateau region changes to between 3 to 4.5 V. The hysteresis seen between charge and discharge is greater than seen in Figure 7b, and there is a much larger charge imbalance seen over the first few cycles. The discharge curve shows a similar pattern to that seen in Figure 7a over the first few cycles with a plateau seen between 4.5 and 3 V. However, after ~4 cycles 80% of the discharge capacity is delivered between 3.5 and 2.25 V; this is possibly indicating an increased resistance in the material resulting from continued cycling and therefore an increased IR drop.

The material synthesized at 700 °C has a far greater retention of capacity per cycle than the 950 °C material; this is shown in Figure 8. The 950 °C material shows an initial discharge capacity of 130 mA h g^{-1} which decreases to less than 20 mA h g^{-1} after 13 cycles. The 700 °C material which was cycled between 2 and 4.2 V had an initial discharge capacity of 146 mA h g^{-1} which decreased to 121 mA h g^{-1} by the 31st cycle. This corresponds to a percentage of capacity retention per cycle of 99.45%. This same material when cycled between 2 and 4.5 V shows an initial capacity of 186 mA h g^{-1} which has dropped to only 122 mA h g^{-1} and relates to a percentage of capacity retention per cycle of 98.9%. Typical values reported in the literature for capacity retention per cycle are 99.9 (initial capacity 190 mA h g^{-1}),[15] 99.7 (200 mA h g^{-1}),[13] and 99.6% (145 mA h g^{-1}).[33]

SEM Images on Bulk Samples. Sample morphology and particle size was investigated as a possible reason for the improved

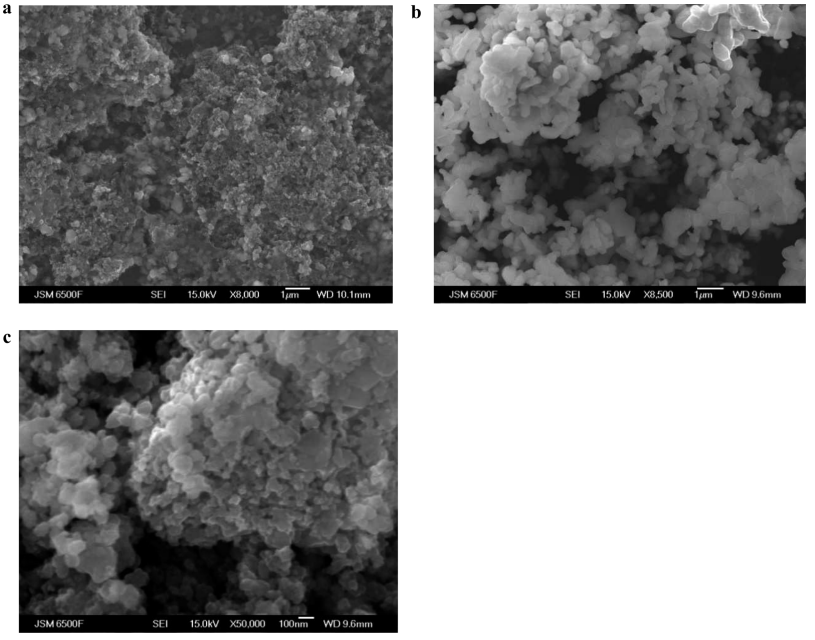

Figure 9. SEM images of $LiNi_{1/3}Co_{1/3}Mn_{1/3}O_2$ prepared from nitrate only precursor calcined at (a) 700 and (b) 900 °C at 8000× magnification. Shown in (c) is the 50,000× magnification SEM image of $LiNi_{1/3}Co_{1/3}Mn_{1/3}O_2$ prepared from nitrate only precursor at 700 °C.

performance of the 700 °C samples. The broadening of the peaks in the XRD data has already indicated a reduction in particle size. To confirm this effect high resolution SEM images were recorded for the 700 and 950 °C nitrates only preparations shown in Figure 9.

In Figure 9 the particle size is approximately 100 and 500 nm for the 700 and 950 °C synthesis temperatures, respectively. The morphology of the particles is also temperature dependent, the 700 °C preparation shows sharp faceted crystals, whereas the 950 °C preparations show rounded crystal edges, and large agglomerates. However, although in this work the 700 °C preparation performs best, the particle morphology of 950 °C material is more consistent with those preparations reported within the literature (also prepared at 950 °C), particularly the material prepared by Shaju et al.[15] who report the highest capacity, rate capability, and capacity retention on cycling.

The above findings highlight the importance of sample morphology in obtaining improved capacity retention. However, the very low temperatures for optimal synthesis reported here do not typically match those from the literature. Several studies have been undertaken to try and optimize the synthesis conditions all involving different synthetic routes and all concluding different optimal synthesis temperatures (800,[34] 850,[18] 900,[19] 950,[15] 1000[33]), times and precursors. It is therefore difficult to make any statements about this material in general, and the materials performance is clearly sensitive to the preparation routes.

The results show a clear correlation between good cyclability and small particle size. This concurs with the generally accepted argument that capacity loss on cycling is due to particle fracture, which is in turn due to the stress caused by inhomogeneity of strain within single crystallites. The latter effect is reduced in small particles, hence the better cycling.

CONCLUSIONS

Our previously described method for high-throughput synthesis of lithium battery cathodes has been modified to incorporate a graded calcination temperature. The new method was then used to compare a number of different precursors while simultaneously varying the calcination temperature in a two-dimensional array. This method can easily be applied to future investigations of new systems.

A low temperature preparation of $LiNi_{1/3}Co_{1/3}Mn_{1/3}O_2$ from nitrate precursors gave a good electrochemical performance within a limited potential range. A low capacity loss on cycling was correlated with the smaller particle size obtained at the lower calcination temperature.

AUTHOR INFORMATION

Corresponding Author

*E-mail: mrr100@soton.ac.uk. Phone: 02380 594114.

ACKNOWLEDGMENT

The authors are grateful for financial support (M.R.R.) from the EPSRC (GR/S27238/01 ADLiB project) and The University of Southampton Combinatorial Centre of Excellence (GR/M88365/01 JIF award).

REFERENCES

(1) R. A..Potyrailo, W. F..Maier *Combinatorial and Highthroughput Discovery and Optimisation of Catalysts and Materials*; Taylor and Francis Group: Abingdon, U.K., 2007.

(2) Spong, A. D.; Vitins, G; Guerin, S; Hayden, B. E.; Russell, A. E.; Owen, J. R. Combinatorial arrays and parallel screening for positive electrode discovery. *J. Power Sources* **2003,** *119*, 778–783.

(3) Cumyn, V. K.; Fleischauer, M. D.; Hatchard, T. D.; Dahn, J. R. Design and testing of a low-cost multichannel pseudopotentiostat for quantitative combinatorial electrochemical measurements on large electrode arrays. *Electrochem. Solid-State Lett.* **2003,** *6*, E15–E18.

(4) Chen, Z; Dahn, J. R. Reducing Carbon in LiFePO4/C Composite Electrodes to Maximize Specific Energy, Volumetric Energy, and Tap Density. *J. Electrochem. Soc.* **2002,** *149*, A1184.

(5) Fleischauer, M. D.; Dahn, J. R. Combinatorial investigations of the Si-Al-Mn system for Li-ion battery applications. *J. Electrochem. Soc.* **2004,** *151*, A1216–A1221.

(6) Fleischauer, M. D.; Obrovac, M. N.; McGraw, J. D.; Dunlap, R. A.; Topple, J. M.; Dahn, J. R. Al-M (M = Cr, Fe, Mn, Ni) thin-film negative electrode materials. *J. Electrochem. Soc.* **2006,** *153*, A484–A491.

(7) Devenney, M.; Donne, S. W.; Gorer, S. Application of combinatorial methodologies to the synthesis and characterization of electrolytic manganese dioxide. *J. Appl. Electrochem.* **2004,** *34*, 643–651.

(8) Fujimoto, K.; Takada, K.; Sasaki, T.; Watanabe, M. Combinatorial approach for powder preparation of pseudo-ternary system LiO0.5-XTiO2 (X: FeO1.5, CrO1.5 and NiO). *Appl. Surf. Sci.* **2004,** *223*, 49–53.

(9) Armand, M.; Gauthier, M.; Magnan, J. F.; Ravet, N. U.S. Patent 033,360 (2004), 2004.

(10) Padhi, A. K.; Nanjundaswamy, K. S.; Goodenough, J. B. Phospho-olivines as positive-electrode materials for rechargeable lithium batteries. *J. Electrochem. Soc.* **1997,** *144*, 1188–1194.

(11) Padhi, A. K.; Nanjundaswamy, K. S.; Masquelier, C.; Okada, S.; Goodenough, J. B. Effect of structure on the Fe3+/Fe2+ redox couple in iron phosphates. *J. Electrochem. Soc.* **1997,** *144*, 1609–1613.

(12) Potyrailo, R. A.; Surman, C.; Morris, W. G. Combinatorial screening of polymeric sensing materials using RFID sensors: combined effects of plasticizers and temperature. *J. Comb. Chem.* **2009,** *11*, 598–603.

(13) Ohzuku, T.; Makimura, Y. Layered lithium insertion material of LiCo1/3Ni1/3Mn1/3O2 for lithium-ion batteries. *Chem. Lett.* **2001,** *7*, 642–643.

(14) Yabuuchi, N.; Ohzuku, T. Novel lithium insertion material of LiCo1/3Ni1/3Mn1/3O2 for advanced lithium-ion batteries. *J. Power Sources* **2003,** *119*, 171–174.

(15) Shaju, K. M.; Bruce, P. G. Macroporous Li(Ni1/3Co1/3Mn1/3)O-2: A high-power and high-energy cathode for rechargeable lithium batteries. *Adv. Mater.* **2006,** *18*, 2330.

(16) Ohzuku, T.; Ariyoshi, M.; Makimura, Y.; Yabuuchi, N.; Sawai, K. Materials strategy for advanced lithium-ion (shuttlecock) batteries: lithium nickel manganese oxides with or without cobalt. *Electrochemistry* **2005,** *73*, 2–11.

(17) Shaju, K. M.; Rao, G. V.; Chowdari, B. V. Performance of layered Li(Ni1/3Co1/3Mn1/3)O-2 as cathode for Li-ion batteries. *Electrochim. Acta* **2002,** *48*, 145–151.

(18) Luo, X. F.; Wang, X. Y.; Liao, L.; Wang, X. M.; Gamboa, S.; Sebastian, P. J. Effects of synthesis conditions on the structural and electrochemical properties of layered Li[Ni1/3Co1/3Mn1/3]O-2 cathode material via the hydroxide co-precipitation method LIB SCITECH. *J. Power Sources* **2006,** *161*, 601–605.

(19) Zhang, L. Q.; Wang, X. Q.; Muta, T.; Li, D. C.; Noguchi, H.; Yoshio, M.; et al. The effects of extra Li content, synthesis method, sintering temperature on synthesis and electrochemistry of layered LiNi1/3Mn1/3Co1/O-3(2). *J. Power Sources* **2006,** *162*, 629–635.

(20) Kim, Y.; Kim, H. S.; Martin, S. W. Synthesis and electrochemical characteristics of Al2O3-coated LiNi1/3Co1/3Mn1/3O2 cathode materials for lithium ion batteries. *Electrochim. Acta* **2006,** *52*, 1316–1322.

(21) Sun, Y. K.; Cho, S. W.; Lee, S. W.; Yoon, C. S.; Amine, K. AlF3-coating to improve high voltage cycling performance of Li[Ni1/3Co1/3Mn1/3]O2 cathode materials for lithium secondary batteries. *J. Electrochem. Soc.* **2007,** *154*, A168–A172.

(22) Shin, H. S.; Shin, D.; Sun, Y. K. Improvement of electrochemical properties of Li[Ni0.4Co0.2Mn((0.4-x))Mg-x]O-2-F-y(y) cathode materials at high voltage region. *Electrochim. Acta* **2006,** *52,* 1477–1482.

(23) Ye, S. Y.; Xia, Y. Y.; Zhang, P. W.; Qiao, Z. Y. Al, B, and F doped LiNi1/3Co1/3Mn1/3O2 as cathode material of lithium-ion batteries. *J. Solid State Electrochem.* **2007,** *11,* 805–810.

(24) Thackeray, M. M.; Kang, S. H.; Johnson, C. S.; Vaughey, J. T.; Benedek, R.; Hackney, S. A. Li2MnO3-stabilized LiMO2 (M = Mn, Ni, Co) electrodes for lithium-ion batteries. *J. Mater. Chem.*. **2007,** *17,* 3112–3125.

(25) Henderson, S.; Armstrong, J.; Hector, A.; Weller, M. High-throughput methods to optically functional oxide and oxide nitride materials. *J. Mater. Chem.* **2005,** *15,* 1528.

(26) Roberts, M. R.; Spong, A. D.; Vitins, G.; Owen, J. R. High throughput screening of the effect of carbon coating in LiFePO4 electrodes. *J. Electrochem. Soc.* **2007,** *154,* A921–A928.

(27) Johns, P.; Roberts, M.; Wakizaka, Y.; Sanders, J. H.; Owen, J. How the electrolyte limits fast discharge in nanostructured batteries and supercapacitors. *Electrochem. Commun.* **2009,** *11,* 2089–2092.

(28) Le Gall, T.; Reiman, K. H.; Grossel, M. C.; Owen, J. R. Poly (2, 5-dihydroxy-1, 4-benzoquinone-3, 6-methylene): a new organic polymer as positive electrode material for rechargeable lithium batteries. *J. Power Sources* **2003,** *119,* 316–320.

(29) Weller, M. *Inorganic Materials Chemistry*; Oxford University Press: New York, 1994; p 25.

(30) West, A. R. *Solid State Chemistry And its Applications*; John Wiley and Sons Ltd: New York, 1984; p 174.

(31) Roberts, M.; Vitins, G.; Denuault, G.; Owen, J. High Throughput Electrochemical Observation of Structural Phase Changes in LiFe1-xMnxPO4 during Charge and Discharge. *J. Electrochem. Soc.* **2010,** *157,* A381.

(32) Whittingham, M. S. Lithium batteries and cathode materials. *Chem. Rev.* **2004,** *104,* 4271–301.

(33) Patoux, S.; Doeff, M. Direct synthesis of LiNi1/3Co1/3Mn1/3O2 from nitrate precursors. *Electrochem. Commun.* **2004,** *6,* 767–772.

(34) Guo, J.; Jiao, L.; Yuan, H.; Li, H.; Zhang, M.; Wang, Y. Effect of synthesis condition on the structural and electrochemical properties of Li[Ni1/3Mn1/3Co1/3]O2 prepared by the metal acetates decomposition method. *Electrochim. Acta* **2006,** *51,* 3731–3735.

(35) Yin, S.; Rho, Y.; Swainson, I.; Nazar, L. F. X-ray/Neutron Diffraction and Electrochemical Studies of Lithium De/Re-Intercalation in Li1-xCo1/3Ni1/3Mn1/3O2 (x = 0 → 1). *Chem. Mater.* **2006,** *18,* 1901.